Insights into the origin of the first sharp diffraction peak in amorphous silica from an analysis of chemical and radial ordering

Parthapratim Biswas [1,*] Devilal Dahal,[1,†] and Stephen R. Elliott[2,3,‡]

[1]*Department of Physics and Astronomy, University of Southern Mississippi, Hattiesburg, Mississippi 39406, USA*
[2]*Physical and Theoretical Chemistry Laboratory, University of Oxford, Oxford OX1 3QZ, United Kingdom*
[3]*Department of Chemistry, University of Cambridge, Cambridge CB2 1EW, United Kingdom*

The structural origin of the first sharp diffraction peak (FSDP) in amorphous silica is studied by analyzing chemical and radial ordering of silicon (Si) and oxygen (O) atoms in binary amorphous networks. The study shows that the chemical order involving Si–O and O–O pairs play a major role in the formation of the FSDP in amorphous silica. This is supplemented by small contributions arising from the relatively weak Si–Si correlations in the Fourier space. A shell-by-shell analysis of the radial correlations between Si–Si, Si–O, and O–O atoms in the network reveals that the position and the intensity of the FSDP are largely determined by atomic pair correlations originating from the first two/three radial shells on a length scale of about 5–8 Å, whereas the fine structure of the intensity curve in the vicinity of the FSDP is perturbatively modified by atomic correlations arising from the radial shells beyond 8 Å. The study leads to a simple mathematical relationship between the position of the radial peaks (r_k) in the partial pair-correlation functions and the diffraction peaks (Q_k) that can be used to obtain approximate positions of the FSDP and the principal peak. The results are complemented by numerical calculations and an accurate semi-analytical expression for the diffraction intensity obtained from the partial pair-correlation functions of amorphous silica for a given radial shell.

I. INTRODUCTION

Amorphous silica (a-SiO$_2$) is one of the most extensively studied noncrystalline solids. While the local structure of amorphous silica is well described in terms of the approximate tetrahedral arrangement of Si and O atoms leading to short-range ordering (SRO) in the network, the medium-range order (MRO) in a-SiO$_2$ is relatively less understood as far as the real-space ordering of the atoms is concerned [1–6]. The SRO in network glasses is readily reflected in the pair-correlation functions (PCF) and the bond-angle distributions. The appearance of the MRO in real space is much more subtle and difficult to gauge, however. In a-SiO$_2$, the MRO is often associated with the relative position and orientation of Si[O$_4$]$_{\frac{1}{2}}$ tetrahedra in forming a continuous random network. In the presence of short-range ordering, driven by local chemistry and geometry, these structural motifs connect with the neighboring motifs in such a way that the resulting network exhibits atomic correlations on a nanometer length scale [7]. Although these intermediate correlations reside in the PCF in a rather obscure way [8,9], their presence is particularly evident in the Fourier space. The radial correlations in the PCF, extending up to a few nanometers in some glasses, can manifest in the form of a sharp diffraction peak in the region of 1–2 Å^{-1} in the Fourier space. For a-SiO$_2$, this leads to the presence of a sharp

peak at $Q_1 = 1.5$ Å^{-1}, also known as the first sharp diffraction peak (FSDP), which serves as a key indicator of the presence of MRO in the network.

The FSDP in glasses has been studied extensively via x-ray and neutron diffraction experiments [10–19], and computational modeling of glasses in simulation studies [9,20–25]. Although these studies have produced a wealth of structural information on glasses and established that the FSDP is a nearly universal feature of network glasses, a definitive understanding of the origin of the FSDP, and its thermodynamic behavior with respect to pressure and temperature [10–12,16,19,26], in terms of the real-space ordering of atoms on the medium-range length scale is yet to be achieved.

In the past decades, several explanations for the possible origin of the FSDP in network glasses were proposed in the literature [14,21,22,27–29]. Among these explanations, the viewpoints presented by Gaskell and Wallis [27] and Elliott [21,22] are most noteworthy. Following Gaskell and Wallis, the FSDP in network glasses is often attributed to the presence of diffuse quasi-Bragg planes, which are assumed to be separated by a distance of the order of $d_1 = 2\pi/Q_1$ in real space. These quasi-Bragg planes are believed to originate from fluctuations of order, which produce a strong scattering in the region of 1–2 Å^{-1} in most glasses. For a-SiO$_2$, this translates into a value of $d_1 \approx 4$ Å and experimental data obtained from high-resolution electron microscope (HREM) images of a-SiO$_2$ appear to support the existence of these quasi-Bragg planes [27]. The presence of quasi-Bragg planes in a-SiO$_2$ was also reported in a simulation study by Uchino *et al.*[24], who employed a real-reciprocal space analysis of

*Corresponding author: partha.biswas@usm.edu

†devilal.dahal@usm.edu

‡sre1@cam.ac.uk

the pair-correlation function of a-SiO$_2$ by using a continuous wavelet transform technique.

An alternative view is provided by Elliott [3,21]. In this approach, the chemical ordering of interstitial voids—associated with cation-centered structural motifs or clusters—in network glasses plays a central role in the formation of the FSDP. The author has shown that the FSDP in network glasses can be regarded as a prepeak in the concentration-concentration partial structure factor (obtained in the Bhatia-Thornton formalism [30]) $S_{cc}(Q)$ originating from low-atomic-occupancy zones or voids in cluster+void networks. A direct application of this cluster+void model leads to the position of the FSDP in a-SiO$_2$ near 1.52 Å^{-1} [21], which includes a corrective factor due to Blétry [31]. The pressure and temperature dependence of the FSDP can be successfully described using this model for most AX_2-type (A = Si, Ge; X = O, S, Se) network glasses. Although some authors [14] have disputed the applicability of the cluster+void model for a-SiO$_2$, experimental studies on densified a-SiO$_2$ do indicate that interstitial voids play an important part in the formation of the FSDP and its behavior upon change of pressure and temperature [16,26]. It may be noted that these two seemingly different explanations are not totally unrelated to each other due to the presence of interstitial voids and hence the resulting fluctuations of the atomic density that can lead to strong scattering in the region of 1–2 Å^{-1}.

In this paper, we employ a simple but deftly implemented approach in real space to understand and gain deeper insights on the origin and structure of the FSDP in a-SiO$_2$. Although our paper is focused on a-SiO$_2$, the approach employed here is very general in nature and it can be applied to any network-forming amorphous solids, including amorphous silicon [9]. In our approach, we shall address the problem from a real-space point of view and demonstrate that the position of the FSDP (and the principal peak [32] as well) can be explained from a knowledge of the partial PCFs and their relationship with the corresponding structure factors. In particular, we shall show that the FSDP corresponds to the minimal value of Q for which radial correlations originating from distant atomic shells in real space interfere constructively to produce a strong intensity peak in the region of 1–2 Å^{-1}. A direct consequence of this approach is that it can explain why certain atomic pairs (for example, Si–Si pairs in a-SiO$_2$) contribute very little to the FSDP, due to cancellation effects of contributions from neighboring radial shells. The key purpose of this study is to develop a quantitative approach for characterizing the radial contributions (of atomic correlations) from distant atomic shells to the FSDP, and to examine the relevant length scale(s) associated with these contributions.

The rest of the paper is presented as follows. In Sec. II, we discuss the computational method employed to generate the structure of a-SiO$_2$, using a combination of Reverse Monte Carlo and first-principles simulations. Section III discusses the results. Starting with the validation of the models, the positions of the FSDP and the principal peak are obtained by developing a simple ansatz from a knowledge of the partial PCFs. This is followed by a discussion on the origin of the FSDP and the principal peak, with particular emphasis on the contribution arising from individual radial shells of Si–Si, Si–O, and O–O pairs in real space. The results are
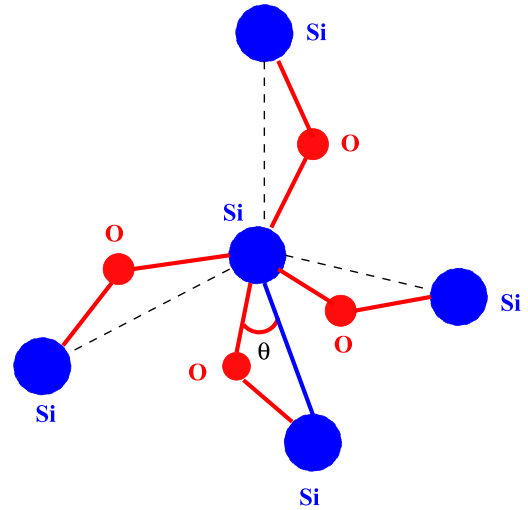

FIG. 1. Construction of an initial configuration of a-SiO$_2$ from a tetrahedral model of amorphous silicon (blue) by introducing oxygen atoms (red) near the center of Si–Si bonds in the network. Each oxygen atom makes an angle θ of about 10–25° with its nearest Si–Si bond as indicated in the diagram.

verified numerically and semi-analytically. The latter is achieved by deriving an accurate semi-analytical expression for the diffraction intensity originating from a given radial shell in the Gaussian approximation. The conclusions are presented in Sec. IV.

II. COMPUTATIONAL METHOD

The starting point of this study is to construct a model of a-SiO$_2$ using a combination of reverse Monte Carlo (RMC) [33,34] and *ab initio* molecular dynamics (AIMD) simulations [35–37]. To this end, we begin with a 216-atom model of amorphous silicon (a-Si) with no coordination defects. This initial "seed" model is used as a framework structure, which can be augmented by adding oxygen atoms in the network. The generation of a-SiO$_2$ models in our approach thus consists of the following steps [34,37]:

(i) The first step involves incorporation of oxygen atoms in a 216-atom a-Si network. For a given Si–Si bond, an oxygen atom was placed close to (but not at) the center of the bond so that the resulting Si–O–Si bond angle lay between 130 to 160°. This was achieved by generating a random unit vector that made an angle $\theta = 10-25°$ with the Si–Si bond direction. An oxygen atom was then placed at a distance of approximately half of the Si–Si bond length along the unit vector. Care was taken to ensure that oxygen atoms were always placed either to the left or to the right of the four Si–Si bonds associated with a central silicon atom in order to construct an initial configuration as close as possible to the a-SiO$_2$ geometry. This is illustrated in Fig. 1, where four oxygen atoms can be seen to appear on the right of the Si–Si bonds (viewing clockwise from above) originating from the central Si atom to produce an approximate tetrahedral unit of Si[O$_4$]$_{\frac{1}{2}}$. The procedure was repeated for all Si–Si bonds in the network. The atomic positions in the resulting structure were then scaled by adjusting the length of the cubic simulation

cell in order to match the mass density of the model with the experimental density of 2.2 g cm^{-3} [38] of a-SiO$_2$.

(ii) Having included the correct stoichiometry, approximate chemical ordering, topology, and geometry of the a-SiO$_2$ structure in the network, the resulting model was subjected to RMC simulations in the second step. The RMC simulation proceeds by matching the experimental neutron-weighted total structure factor of a-SiO$_2$ with that calculated for the model. This is accomplished by constructing a cost functional that comprises the structure-factor data and constraints on O–Si–O bond angles and their standard deviation so that the bond-angle distribution, imposed via selective addition of oxygen atoms in the first step, cannot deviate considerably from the approximate tetrahedral distribution of O–Si–O bond angles during RMC evolution.

During RMC simulations, a proposed RMC move is accepted with Metropolis probability, $P = \min[1, e^{-\beta \Delta \mathcal{E}}]$, where β is an optimization parameter and $\Delta \mathcal{E} = \mathcal{E}_f - \mathcal{E}_i$ is the difference between the final value and the initial value of the cost functional for a single RMC move. As in MD simulations, an annealing protocol is implemented in the RMC runs by slowly varying the parameter β with RMC steps. Starting with a small value of β, the value is gradually increased at a regular interval and the configuration is relaxed for each value of β. Since there exists no real energy scale (or temperature) associated with a cost functional in RMC simulations, one can directly vary β with RMC steps without invoking a temperature. It is the variation of β with RMC steps that plays an equivalent role of annealing (in MD simulations) to facilitate structural formation in the network including short-range and medium-range ordering during RMC evolution. Detailed discussions on the generation of amorphous structures using RMC and post-RMC simulations are given by McGreevy [33] and others [39–46].

(iii) The final step of the method involves thermalization of the RMC-obtained structure, which is followed by geometry relaxations using density functional theory (DFT). This is to ensure that the structural information enforced into the system in the last two steps is consistent with "thermodynamic" equilibrium or a strong minimum, as determined by total energy and forces from DFT calculations. The thermalization was done by conducting AIMD simulations in canonical ensembles at 600 K for a total simulation time of 5 ps using the code SIESTA [47]. The choice of a relatively short AIMD-relaxation time of 5 ps and a temperature of 600 K is guided by our desire to ensure that important structural features of the RMC solution, which are incorporated during the RMC evolution, do not wash away upon AIMD relaxations. A long AIMD run can strip off or degrade the characteristic features of the RMC solution, leaving behind essentially an AIMD-relaxed configuration. One may thus view the short MD relaxation as a possible corrective measure to maintain the thermodynamic stability of the solution and the RMC method as a key driver to propagate the solution on the multi-dimensional cost-functional surface so that the solution does not deviate far from the actual potential-energy surface of a-SiO$_2$. A temperature below 400 K might not be very effective for short relaxations to achieve the stated goal above, whereas a high temperature (say, above 800 K) may adversely affect the RMC features of the solution. For a lower temperature, one may

need to use a somewhat longer relaxation time than 5 ps, albeit at a high computational cost of AIMD runs, and vice versa. SIESTA employs atom-centered numerical basis functions to solve the Kohn-Sham equation using the self-consistent field approximation within the framework of density functional theory (DFT). The norm-conserving pseudopotentials for silicon and oxygen atoms in the Troullier-Martins form [48] were used to describe the electron-ion interactions, and the exchange-correlation energy of the system was computed in the generalized gradient approximation (GGA) [49]. The total energy of the thermalized models was further minimized by employing the conjugate gradient (CG) method using *ab initio* forces and total energy obtained from SIESTA. Throughout the calculations, we used double-zeta basis functions. The CG relaxation continued until the magnitude of the total force on each atom was less than or equal to 0.01 eV/Å.

To study the origin and structure of the FSDP and the principal peak in a-SiO$_2$ by analyzing the radial pair correlations between constituent atoms, we assume that the disordered system is isotropic and homogeneous in nature. Following Elliott [50], the reduced scattering intensity (I_r) for such a system, consisting of N atoms or scatterers, can be written as

$$I_r = \frac{Q}{\langle f \rangle^2} \left[\frac{I}{N} - \langle f^2 \rangle \right]$$

$$= \int_0^\infty 4\pi \rho_0 r [g(r) - 1] \sin Qr \, dr, \qquad (1)$$

where $g(r)$ is the total atomic pair-correlation function (PCF), ρ_0 is the average number density of the system, and I is the total intensity. The symbol $\langle f^n \rangle$ (for $n = 1, 2$) stands for the concentration-weighted average value of the nth moment of the scattering factor f. Writing

$$g(r) = \sum_{ij} \frac{c_i c_j f_i f_j}{\langle f \rangle^2} g_{ij}(r) = \sum_{ij} \omega'_{ij} \, g_{ij}(r) \qquad (2)$$

in terms of the partial PCFs, $g_{ij}(r)$, and noting that c_i and f_i are the atomic fraction and the scattering factor of atoms of type i, respectively, Eq. (1) can be expressed as [50]

$$\frac{I}{N\langle f^2 \rangle} - 1 = \sum_{ij} \frac{c_i c_j f_i f_j}{\langle f^2 \rangle} [I_{ij}(Q) - 1]$$

$$= \sum_{ij} \omega_{ij} [I_{ij}(Q) - 1]. \qquad (3)$$

In Eq. (3), I_{ij} is the partial interference function

$$I_{ij}(Q) = 1 + \frac{1}{Q} \int_0^\infty 4\pi \rho_0 \, r [g_{ij}(r) - 1] \sin Qr \, dr$$

and $g_{ij}(r)$ is the partial PCF between atoms of type i and type j. It may be noted that the coefficients ω_{ij} and ω'_{ij} are close to each other but not identical because of the use of different denominators, $\langle f^2 \rangle$ and $\langle f \rangle^2$, respectively, in their definition, and $\sum_{ij} \omega'_{ij} = 1$. For an elemental system, Eq. (3) reduces to the well-known expression for the static structure factor

$$S(Q) = \frac{I}{Nf^2} = 1 + \frac{4\pi \rho_0}{Q} \int_0^\infty r [g(r) - 1] \sin Qr \, dr.$$
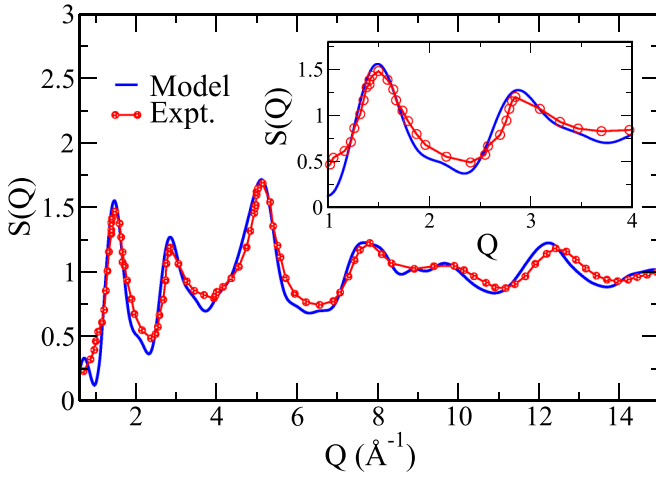
FIG. 2. The neutron-weighted static structure factor of a-SiO$_2$ obtained from averaging over two 648-atom models (blue line) and experiments (red circles) [11]. The inset shows a magnified view of the FSDP and the principal peak, at 1.5 and 2.8 Å^{-1}, respectively.
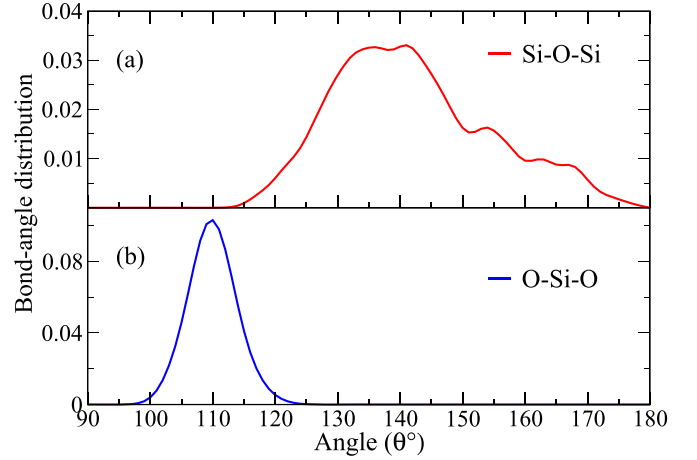

FIG. 3. The bond-angle distributions associated with: (a) Si–O–Si angles and (b) O–Si–O angles. The average values of Si–O–Si and O–Si–O are 141.5° and 109.5°, respectively. The corresponding standard deviations are found to be 12.5° and 3.5°.

For our purpose, we rewrite Eq. (3) as

$$S(Q) - 1 = F(Q) = \sum_{ij} \omega_{ij}(I_{ij}(Q) - 1) = \sum_{ij} F_{ij},$$

where

$$F_{ij}(Q) = \frac{4\pi \rho_0 \omega_{ij}}{Q} \int_0^\infty r \left[g_{ij}(r) - 1\right] \sin Qr \, dr. \qquad (4)$$

The upper limit of the integral in Eq. (4) is generally truncated and replaced by a finite cutoff value of R_c. The latter is usually taken to be the half of the cubic simulation cell length or a value of r for which $g_{ij}(r \geqslant R_c) = 0$. The R_c value for the present models is about 10.7 Å. For neutron scattering, the expressions in this section are valid provided that one replaces the scattering factors f_i by the corresponding neutron-scattering lengths b_i for s-wave scattering [51,52]. The values of b_{Si} and b_O are given by 4.149 and 5.803 fm, respectively.

III. RESULTS AND DISCUSSION

A. Validation of structural models

Before addressing the results, we briefly examine the static structure factor of the model and compare the results with those from experiments in order to validate the model used in our calculations. For binary a-SiO$_2$, it suffices to examine the distributions of Si–O–Si and O–Si–O bond angles, and the full structure factor for the purpose of validating a model.

Figure 2 shows the neutron-weighted static structure factor $S(Q)$ obtained from two 648-atom models of a-SiO$_2$. Here, $S(Q)$ has been computed following the Faber-Ziman approach [53] using Eq. (4). The corresponding experimental data for a-SiO$_2$ from neutron diffraction measurements by Susman *et al.*[11] are also included in the figure. It is evident from the plots that the computed and experimental values agree well in the scattering-vector region from 0.6 to 15 Å^{-1}. A small deviation below 1 Å^{-1} can be attributed to finite-size effects on $G(r)$ obtained from small models. The presence

of numerical noise in $G(r)$ at large distances can make $S(Q)$ particularly sensitive in the small-angle region of $Q < 1$ Å^{-1} [54] for small finite-size models.

The FSDP and the principal peak are found to be at 1.5 and 2.8 Å^{-1}, respectively, which are shown in the figure more closely as an inset along with their experimental counterparts. The position of the FSDP at 1.5 Å^{-1} is also consistent with those from the x-ray diffraction measurements by Tan and Arndt [26] and MD simulations reported in the literature by others [20,23]. The average value of the Si–O bond length is found to be 1.64 ± 0.013 Å, which is a bit larger than the experimental value of 1.61 ± 0.09 Å [14,55] and 1.62 ± 0.08 Å from first-principles MD simulations reported in the literature [20,23,37]. Likewise, the average nearest-neighbor distances between Si–Si and O–O pairs are found to be 3.14 ± 0.14 Å and 2.63 ± 0.06 Å. These values compare well with the average Si–Si distance of 3.1 Å and the average O–O distance of 2.64 Å obtained from classical MD simulations [20,56], and 3.12 Å and 2.65 Å, respectively, from *ab initio* MD simulations [37]. The computed values are close to the experimental values of Si–Si and O–O distance of 3.08 ± 0.1 and 2.63 ± 0.089 Å, respectively, which were obtained by Johnson *et al.*[55] by assuming that the radial peaks are symmetric and can be fitted by a Gaussian function [55].

Turning to bond angles, the O–Si–O and Si–O–Si angles play a critical role in building the local structure and topology of a-SiO$_2$, and the connectivity between SiO$_{4/2}$ tetrahedra in the network. These two angles provide the relative shape and orientation of two neighboring SiO$_{4/2}$ tetrahedra that form the structural basis of amorphous silica networks. The distributions of these angles are presented in Fig. 3. The average value of O–Si–O angles in this paper is found to be $109.5 \pm 3.5°$. By contrast, the Si–O–Si angles exhibit a somewhat broader distribution, with an average value of $141.5 \pm 12.5°$. These values match closely with those from earlier MD simulation studies [20,23,37] and experiments [55,57]. In particular, the Car-Parrinello simulations of a-SiO$_2$ using 72-atom models by Sarnthein *et al.*[23] obtained the average values for the
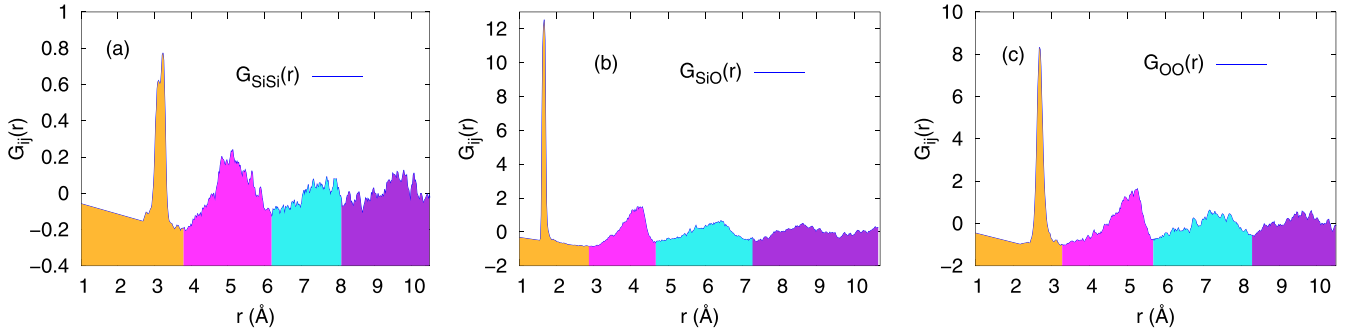
FIG. 4. The neutron-weighted partial reduced PCFs, $G_{ij}(r)$, for: (a) Si–Si, (b) Si–O, and (c) O–O pairs. The first four shells and their radial extent are shown in different colors. The magnitude of Si–Si pair correlations can be seen to be significantly smaller than their Si–O and O–O counterparts, by a factor of about 10.

O–Si–O and Si–O–Si angles to be $109 \pm 6°$ and $136 \pm 15°$, respectively. The corresponding experimental values from x-ray and neutron diffraction are reported to be about $109°$ and 140–$150°$ [55,57].

B. Chemical order in a-SiO$_2$ and the FSDP

In studying the FSDP in network glasses, a question of considerable importance is to what extent the presence of chemical ordering between constituent atoms/species can affect the position and the intensity of the diffraction peak. It is also necessary to ascertain the characteristic length scale of radial correlations that plays the most decisive role in forming the shape of the intensity curve near the FSDP. While it is an established fact that the FSDP originates from medium-range ordering on the length scale of 5–10 Å, a quantitative characterization of the contributions arising from different radial shells and atomic species is still missing in the literature. For a binary a-SiO$_2$ system, this entails examining the role of radial atomic correlations that originate from chemically ordered Si–Si, Si–O, and O–O pairs in forming the FSDP. To address this question, we write

$$F(Q) = \sum_{ij} \omega_{ij}(I_{ij} - 1) = \sum_{ij} F_{ij}(Q)$$

and

$$F_{ij}(Q) = \frac{1}{Q} \int_0^{R_c} G_{ij}(r) \sin Qr\, dr, \qquad (5)$$

where $G_{ij}(r) = 4\pi\rho_0 \omega_{ij} r[g_{ij}(r) - 1]$ is the neutron-weighted reduced atomic pair-correlation function. Equation (5) provides a convenient starting point to determine the contribution to the total FSDP arising from $F_{ij}(Q)$, or its Fourier counterpart $G_{ij}(r)$ in real space.

Figure 4 shows the three neutron-weighted partial PCFs, $G_{ij}(r)$, for a-SiO$_2$. It is apparent from the plots that neutron-weighted Si–Si correlations are considerably weaker than their Si–O and O–O counterparts, with the first two peaks of $G_{\text{SiSi}}(r)$ being about ten times smaller than the corresponding values of $G_{\text{SiO}}(r)$ and $G_{\text{OO}}(r)$. In view of this, it is not inapposite to surmise that the Si–Si correlations may not play a significant role in determining the overall structure of the FSDP. This surmise can be verified by computing $F_{ij}(Q)$ from Eq. (5). Figure 5 shows the contribution to $F(Q)$ from its

three partial components $F_{ij}(Q)$. The major contribution to the FSDP at 1.5 Å^{-1} can be seen to originate from the Si–O correlations, which are followed by the O–O correlations in real space. This statement applies to the principal peak near 2.8 Å^{-1} as well. The presence of weak Si–Si correlations, relative to the magnitude of its Si–O and O–O counterparts, produces an almost flat structure factor in the Fourier space, with two small bulges near 1.5 and 2.7 Å^{-1}. An analysis of Eq. (5), with the aid of Fig. 4 in the next section, will reveal that the first bulge in $F_{\text{SiSi}}(Q)$ near the FSDP arises from the second radial shell of Si–Si correlations [depicted in pink-purple color in Fig. 4(a)], whereas the principal peak in $F_{\text{SiSi}}(Q)$ gets its contribution from both the first and second radial shells of silicon, extending as far as 6 Å.

By contrast, the position of the principal peak in $F(Q)$ (in Fig. 5) is determined by atomic correlations originating from $G_{\text{OO}}(r)$, $G_{\text{SiO}}(r)$, and $G_{\text{SiSi}}(r)$ as follows. The contribution from $G_{\text{OO}}(r)$ produces a strong peak or maximum near 2.8 Å^{-1} in $F_{\text{OO}}(Q)$, whereas $G_{\text{SiO}}(r)$ yields an equally strong minimum near 2.76 Å^{-1} in $F_{\text{SiO}}(Q)$. These two contributions effectively cancel out each other. The resulting intensity
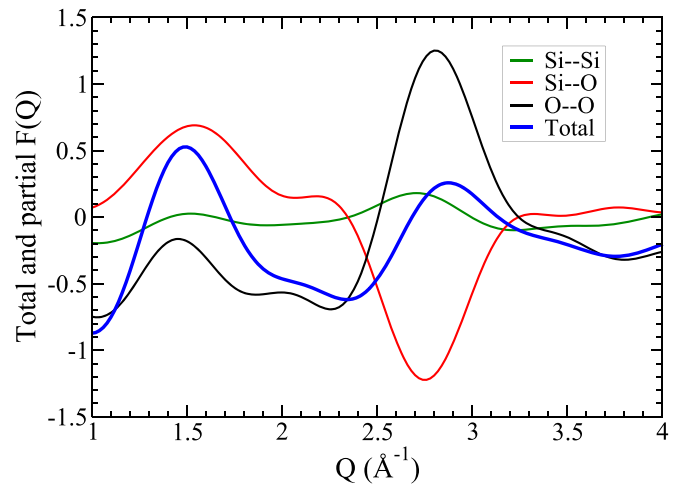

FIG. 5. Neutron-weighted total $F(Q)$ (blue) and its three partial components, $F_{\text{SiSi}}(Q)$, $F_{\text{OO}}(Q)$ and $F_{\text{SiO}}(Q)$, originating from Si–Si (green), O–O (black), and Si–O (red) radial pair correlations, respectively. The FSDP and the principal peak of $F(Q)$ are located at 1.5 and 2.8 Å^{-1}, respectively.

obtained from the sum of $F_{OO}(Q)$, $F_{SiO}(Q)$ and a small positive contribution from $F_{SiSi}(Q)$ near 2.74 Å^{-1} produces the principal peak near 2.8 Å^{-1} in $F(Q)$. It thus appears that the chemical ordering of Si–O and O–O pairs plays an important role by competing with each other in determining the final position and intensity of the principal peak in amorphous silica. On the other hand, the Si–Si pairs provide a small but nontrivial contribution to those originating from Si–O and O–O pairs. Below, we discuss this in detail by developing an ansatz to obtain the approximate positions of the FSDP and the principal peak from Eq. (5).

C. Origin of the FSDP and the principal peak in a-SiO$_2$

The structural origin of the FSDP and the principal peak in a-SiO$_2$ at 1.5 and 2.8 Å^{-1}, respectively, can be intuitively understood from the approximate behavior of Eq. (5) and a knowledge of the partial PCFs. Recently, Dahal *et al.*[9] have provided an explanation of the origin of the FSDP in elemental amorphous systems, such as a-Si, in terms of the radial distribution of atoms in distant atomic shells. For multinary systems, however, the problem is highly nontrivial due to competing contributions arising from several partial components. Further, the position of the FSDP in multinary systems is also influenced by relevant scattering factors that are associated with different atomic species. In the following, we adopt a similar line of argument as in Ref. [9] and generalize the approach for binary amorphous systems. To this end, we rewrite Eq. (5) as

$$F_{ij}(Q) = \int_0^{R_c} r G_{ij}(r) \left[\frac{\sin Qr}{Qr} \right] dr \qquad (6)$$

and postulate—assuming that $rG(r)$ behaves as a narrow distribution or an approximate δ function near the radial peaks—that the maxima (minima) of $F_{ij}(Q)$ should roughly correspond to those values of Q for which $\sin Qr/Qr$ is maximum (minimum), where the values of r are given by the dominant peaks in $rG_{ij}(r)$. Noting that the position of peaks in $G(r)$ and $rG(r)$ are very close to each other [58], and that the maxima (minima) of $(\sin x)/x$ can be expressed in terms of the maxima (minima) of $\sin x$, one can write in the first-order approximation

$$Q_k \approx \frac{(4n \pm 1)\pi}{2r_k} - \frac{2}{(4n \pm 1)\pi r_k}, \quad n = 1, 2, 3, \dots \quad (7)$$

where r_k corresponds to the kth peak in $G_{ij}(r)$ and the plus (minus) sign applies to the maxima (minima). This can be shown by solving the optimality condition, $\cos x = (\sin x)/x$, $(x = Qr)$ for the maxima/minima of $(\sin x)/x$ in terms of the solutions of $\sin x = \pm 1$ or $x_n = (4n \pm 1)\pi/2$ for $n = 0, 1, 2, \dots$ Writing $x = x_n + x'$, where x' is a small correction, one arrives at the first-order correction $x' = -1/x_n$ via power series expansion of $\sin x'$ and $\cos x'$ for small x' in the expression for the optimality condition. For practical purposes, the second term in Eq. (7), which is of the order of 0.1 Å^{-1} [59] for a-SiO$_2$, can be ignored and the approximate values of Q_k then read [60]

$$Q_k \approx \frac{(4n \pm 1)\pi}{2r_k}, \quad n = 1, 2, 3, \dots \quad (8)$$

The validity of the result in Eq. (8) rests on the assumption that the first few peaks in $G(r)$ are well defined and that they progressively decay so that the contribution from distant radial shells/peaks have a decreasing influence on the resultant FSDP and the principal peak in $F(Q)$. For elemental systems, such as a-Si, it has been shown recently that Eq. (8) provides a good estimate of the positions of the FSDP and the principal peak [9]. However, complications can arise for multinary systems where one must take into account not only the contributions from the distant radial shells but also those that originate from different partial components of $G(r)$. Since the contributions from the first few peaks of different $G_{ij}(r)$ could be similar in magnitude but out of phase to varying degrees, the resultant FSDP and the principal peak may or may not appear in the vicinity of Q_k as determined by Eq. (8), due to the cancellation of out-of-phase contributions. This is apparent in Fig. 5, where the position of the principal peak is determined by the sum of the intensity from the neutron-weighted Si–Si, Si–O, and O–O pair correlations in the Fourier space. The intensity from Si–O and O–O correlations cancel each other out for the most part near the principal peak, leaving behind a resulting nontrivial part that combines with the small contribution from Si–Si correlations to determine the final position and the shape of the principal peak at 2.8 Å^{-1}. This observation suggests that a knowledge of the intensity of $F_{ij}(Q)$ near the FSDP and the principal peak can be very useful in determining the exact final position of the peak in multinary systems. We shall delve into this point in the next section. For now, we focus on Eq. (8) to obtain the approximate positions of the FSDP and the principal peak of a-SiO$_2$ with the aid of the neutron-weighted partial PCFs shown in Fig. 4.

Starting with the Si–Si PCF, one notes from Fig. 4 that the positions of the first three peaks (at r_k) are at 3.14, 5.1, and 7.7 Å, respectively. Following Eq. (8), the first radial peak at 3.14 Å is expected to produce a peak at 2.5 Å^{-1} (for $n = 1$) in the Si–Si partial structure factor. Likewise, the second radial peak at 5.1 Å should produce peaks at 1.54 and 2.77 Å^{-1} for $n = 1, 2$, respectively. A similar calculation for the third radial peak at 7.7 Å suggests that a peak should appear at 1.83 Å^{-1} (for $n = 2$) and 2.65 Å^{-1} (for $n = 3$). An examination of the Si–Si partial structure factor in Fig. 5 does confirm the presence of peaks near 1.5 and 2.7 Å^{-1}. In view of this observation, it is apposite to conclude that the Si–Si principal peak near 2.7 Å^{-1} in Fig. 5 gets its contribution mostly from the second and third Si–Si radial shells, whereas only the second shell contributes to the FSDP near 1.5 Å^{-1}. The weak intensity associated with these peaks can be attributed to the relatively small values of neutron-weighted $G_{SiSi}(r)$ (compared to its Si–O and O–O counterparts), the largest absolute value of which over the entire radial range is found to be less than unity in Fig. 4(a).

The foregoing analysis applies to the O–O pairs as well. Figure 4(c) shows that the first three peaks in $G_{OO}(r)$ appear at 2.65, 5.2, and 7.2 Å. Following the same reasoning as before, the first radial peak at 2.65 Å should give rise to a peak at 2.96 Å^{-1} (for $n = 1$) and the second radial peak at 5.2 Å leads to 1.51 and 2.72 Å^{-1} in $F_{OO}(Q)$ for $n=1, 2$, respectively. Similarly, the third peak at 7.2 Å is expected to produce peaks at 1.96 and 2.83 Å^{-1} for $n = 2, 3$, respectively. A comparison of the results with $F_{OO}(Q)$ in Fig. 5 shows that

TABLE I. Approximate positions (Q) of the FSDP (orange cells) and the principal peak (green cells) obtained from the first three radial peaks (r_i) of $G_{SiSi}(r)$ and $G_{OO}(r)$ using Eq. (8). For a given radial peak (r_i) and n, and $K = (4n+1)\pi/2$, the values of $Q = K/r_i$ are listed below in Å^{-1}.

n	K	Si–Si (r_i)			O–O (r_i)		
		3.14 Å	5.1 Å	7.7 Å	2.65 Å	5.2 Å	7.2 Å
1	$5\pi/2$	2.5	1.54	1.02	2.96	1.51	1.1
2	$9\pi/2$	4.5	2.77	1.83	5.33	2.72	1.96
3	$13\pi/2$	6.5	4.0	2.65	7.7	3.93	2.83

the suggested peaks appear near 1.5 and 2.8 Å^{-1}, including a weak quasi-peak near 2 Å^{-1}. Table I lists the approximate positions of the FSDP and the principal peak of $F_{SiSi}(Q)$ and $F_{OO}(Q)$ obtained from using Eq. (8) and the location of the first three radial peaks of $G_{SiSi}(r)$ and $G_{OO}(r)$. The values of Q that contribute to the FSDP and the principal peak are highlighted in Table I in orange and green colors, respectively.

The case for Si–O correlations is a bit confusing, however. In contrast to $F_{SiSi}(Q)$ and $F_{OO}(Q)$, there is no principal peak or maximum in $F_{SiO}(Q)$ but a minimum near 2.8 Å^{-1} (see Fig. 5). The preceding argument works well to determine this minimum using the position of the *minima* obtained from Eq. (8). In particular, the first three peaks of $G_{SiO}(r)$, appearing at 1.65, 4.27, and 6.4 Å, are expected to produce three minima at 2.86 Å^{-1} (for $n = 1$), 2.58 Å^{-1} (for $n = 2$) and 2.7 Å^{-1} (for $n = 3$), respectively. The combined effect of these minima is expected to reflect in $F_{SiO}(Q)$ by producing a strong minimum near 2.8 Å^{-1}. Figure 5 does corroborate this expectation. We shall further confirm this observation using numerical results in Sec. III D. However, the argument appears to fail in locating the FSDP of $F_{SiO}(Q)$ at 1.5 Å^{-1}. Equation (8) suggests that the second radial shell should produce a peak at 1.84 Å^{-1} (for $n = 1$) and the third shell at 1.23 Å^{-1} (for $n = 1$). But none of these positions is close enough to the observed peak at 1.5 Å^{-1} in Fig. 5. Should we consider the fourth radial shell with a peak at 8.6 Å in Fig. 4(b), we get peaks in $F_{SiO}(Q)$ at 0.91 Å^{-1} (for $n = 1$) and 1.64 Å^{-1} (for $n = 2$). But without a knowledge of the intensity of these peaks, it is not clear whether the peaks would coalesce into a single peak at 1.5 Å^{-1} or not. The approximate positions of the maxima and minima of $F_{SiO}(Q)$ obtained from using Eq. (8) for the first four radial peaks are listed in Table II.

The discrepancy observed above concerning the position of the estimated FSDP in $F_{SiO}(Q)$ cannot be satisfactorily explained using the qualitative argument [based on Eq. (8)] presented so far in this section. At this point, it suffices to mention that the anomaly can be resolved by noting that the peak at 1.23 Å^{-1} originating from the third shell interferes constructively with those at 1.84 Å^{-1} from the second shell and at 1.64 Å^{-1} from the fourth shell (see Table II) to produce the FSDP at 1.5 Å^{-1}. In the next two sections, we address this issue by numerical and semi-analytical calculations, and examine the observed behavior of $F_{ij}(Q)$ with reference to neutron-weighted atomic pair correlations arising from individual radial shells of the partial PCFs of a-SiO$_2$.

TABLE II. The approximate location of the maxima (Q_+) and minima (Q_-) in $F_{SiO}(Q)$ obtained from the first four shells using Eq. (8). $K_{(+,-)}$ are given by $(4n \pm 1)\pi/2$ and $Q_\pm = K_{(+,-)}/r_i$. The maxima and minima contributing to the FSDP and the principal minima in $F_{SiO}(Q)$ are indicated in orange and green cells, respectively.

n	$K_{(+,-)}$	Si–O (r_i)							
		1.65 Å	4.27 Å	6.4 Å	8.6 Å	1.65 Å	4.27 Å	6.4 Å	8.6 Å
		Q_+ (maxima)				Q_- (minima)			
1	$\frac{(5,3)\pi}{2}$	4.76	1.84	1.23	0.91	2.86	1.1	0.74	0.54
2	$\frac{(9,7)\pi}{2}$	8.57	3.31	2.21	1.64	6.66	2.58	1.72	1.28
3	$\frac{(13,11)\pi}{2}$	12.37	4.78	3.19	2.37	10.47	4	2.7	2
4	$\frac{(17,15)\pi}{2}$	16.18	6.25	4.17	3.1	14.28	5.52	3.68	2.74

D. Relation between radial correlations, the FSDP and principal peak

In the preceding section, we have seen that the position of the FSDP and the principal peak can be obtained—except for the FSDP in $F_{SiO}(Q)$—from a heuristic argument based on the qualitative behavior of the integral in Eq. (6) and the position of the radial peaks in $G_{ij}(r)$. The argument tacitly assumed that the function $G_{ij}(r)$ can be locally replaced by a sufficiently narrow pair-distribution function or a δ function at the maximum of each radial shell in the zeroth-order approximation. This consideration leads to a reasonable estimate of the position of the maxima/minima in the corresponding partial structure factor, but not the intensity of the peaks/dips. We now examine the accuracy of the position of maxima/minima obtained earlier by numerical calculations and study the radial contribution originating from the individual shells of $G_{ij}(r)$.

To obtain the shell-by-shell contribution from the real-space PCFs, it is convenient to write

$$F_{ij}(Q) = \sum_{\alpha=1}^{s} F_{ij}^\alpha\left(Q; R_\alpha^{ij}, R_{\alpha+1}^{ij}\right)$$

$$= \frac{1}{Q} \sum_{\alpha=1}^{s} \int_{R_\alpha^{ij}}^{R_{\alpha+1}^{ij}} G_{ij}(r) \sin Qr\, dr. \qquad (9)$$

Here, the Greek index α indicates the shell number and the pair of lengths $(R_\alpha^{ij}, R_{\alpha+1}^{ij})$ gives the radial range of the αth shell for the ijth partial PCF, $G_{ij}(r)$. The set $\{R_\alpha^{ij}\}$ is so chosen that it spans the entire radial range of the corresponding PCF from 0 to R_c. Table III lists the pair of values $(R_\alpha^{ij}, R_{\alpha+1}^{ij})$ for

TABLE III. Radial extents of the first four shells in the partial PCF of Si–Si, Si–O, and O–O, as shown in Fig. 4. The pair of numbers within brackets below indicates the range of the αth radial shell in Å.

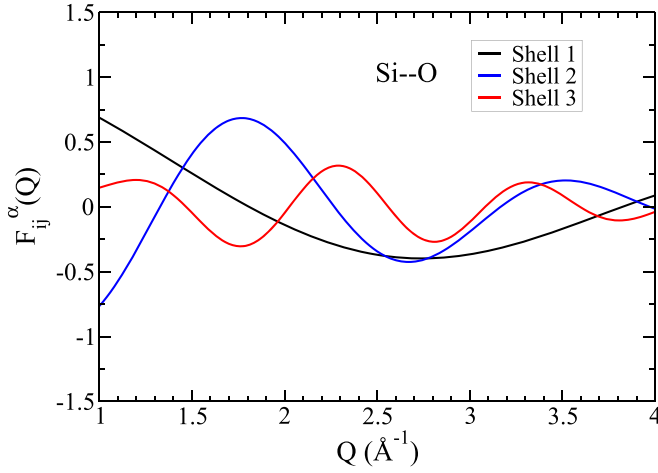| PCF	Shell number			
$\downarrow$	$\alpha = 1$	$\alpha = 2$	$\alpha = 3$	$\alpha = 4$
Si–Si	(0, 3.8)	(3.8, 6.2)	(6.2, 8.1)	(8.1, 10.7)
Si–O	(0, 2.4)	(2.4, 4.6)	(4.6, 7.4)	(7.4, 10.7)
O–O	(0, 3.3)	(3.3, 5.7)	(5.7, 8.3)	(8.3, 10.7)

FIG. 6. The partial structure factors $F_{ij}^\alpha(Q)$ obtained from the first three radial shells (for $\alpha = 1$, 2, and 3) of the Si–O correlation function.

the αth shell of $G_{ij}(r)$. We now use these values of $\{R_\alpha^{ij}\}$ to calculate the radial contribution of the partial PCFs to the intensity of the corresponding $F_{ij}(Q)$ from individual radial shells. Our discussion is mostly confined to Si–O and O–O pair correlations as these two pairs have been found to play a key role in forming the FSDP and the principal peak (cf. Fig. 5). This is followed by a brief mention of Si–Si correlations, which provide small corrections to the intensity of the FSDP/principal peak of the full $F(Q)$.

Figure 6 shows the partial structure factor $F_{SiO}(Q)$ obtained by numerically integrating Eq. (9) for the first three individual shells (for $\alpha = 1$ to 3) using the R_{ij}^α values listed in Table III. The results show that shell 2 produces maxima at 1.8 and 3.52 Å^{-1}, and shell 3 produces maxima at 1.2, 2.3, and 3.32 Å^{-1}. These values are quite close to the estimated values of the maxima listed in Table II from the respective shells. Similarly, the minima from shell 2 and 3 in Fig. 6 correspond to 2.68 Å^{-1}, and 1.76, 2.8, and 3.8 Å^{-1}, respectively. Once again, these values are close to the estimated values of 2.58 Å^{-1}, and 1.72, 2.7, and 3.68 Å^{-1}, respectively, as listed in Table II. By contrast, the contribution from shell 1 provides a monotonic decrease of the intensity with an increasing value of Q near the FSDP. The first shell does not produce any maximum in the region between 1 to 4 Å^{-1} but a minimum at 2.74 Å^{-1}, which is estimated to be 2.86 Å^{-1} in Table II. The latter is very close to the exact numerical value of 2.74 Å^{-1}, when one takes into account the perturbative correction of about 0.128 Å^{-1} for this peak [59].

The observations above suggest that the approximate positions of the maxima (peaks) and minima (dips) in Fig. 6 can be obtained quite accurately from the heuristic argument presented in Sec. III C using Eq. (8). These maxima and minima collectively lead to the formation of the FSDP and the principal minimum in $F_{SiO}(Q)$. The net effect of the contributions from different radial shells to the FSDP and the principal minimum is shown in Fig. 7, where $F_{SiO}(Q)$ obtained from the first two, first three, and first four radial shells are presented. The buildup of the FSDP near 1.5 Å^{-1} is evident from the plots. The resultant $F_{SiO}(Q)$
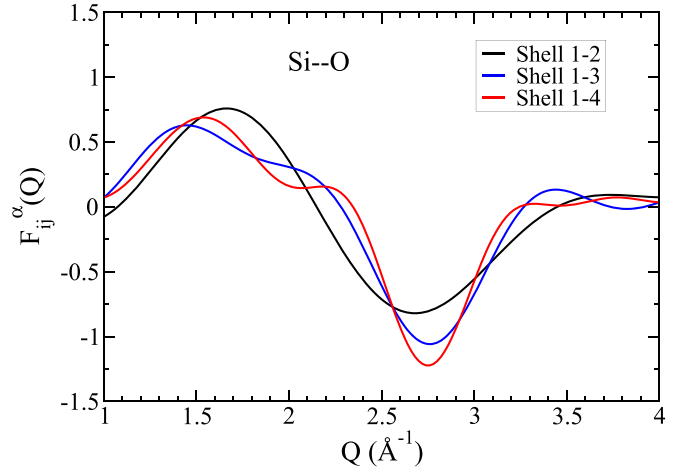

FIG. 7. The formation of the FSDP near 1.5 Å^{-1} and a minimum near 2.8 Å^{-1} in $F_{SiO}(Q)$ originating from the first two, first three, and first four radial shells. The minimum plays an important role in the formation of the principal peak in Fig. 5.

obtained from all radial shells up to 10.7 Å evolves to produce the FSDP near 1.5 Å^{-1} and a minimum near 2.8 Å^{-1}. As stated earlier, there is no principal *peak or maximum* in $F_{SiO}(Q)$ in Fig. 7 but a minimum near 2.8 Å^{-1}. This minimum contributes negatively to form the principal peak in total $F(Q)$ along with the positive contributions from $F_{OO}(Q)$ and $F_{SiSi}(Q)$ near 2.8 Å^{-1}.

A similar analysis of O–O correlations reveals that the approximate locations of the FSDP and the principal peak in $F_{OO}(Q)$ are correctly obtained in Sec. III C. Figure 8 presents the contribution from the first three individual radial shells of $G_{OO}(r)$. The results show the presence of two maxima at 1.42 and 2.82 Å^{-1} originating from the second shell. The corresponding estimated values of the maxima (in Table I) are found to be 1.51 and 2.72 Å^{-1}, respectively. Likewise, the first shell and the third shell each produces a peak at 2.86 and 2.82 Å^{-1}, respectively, which are very close to the estimated values of 2.96 and 2.83 Å^{-1} listed in Table I. The overall effect

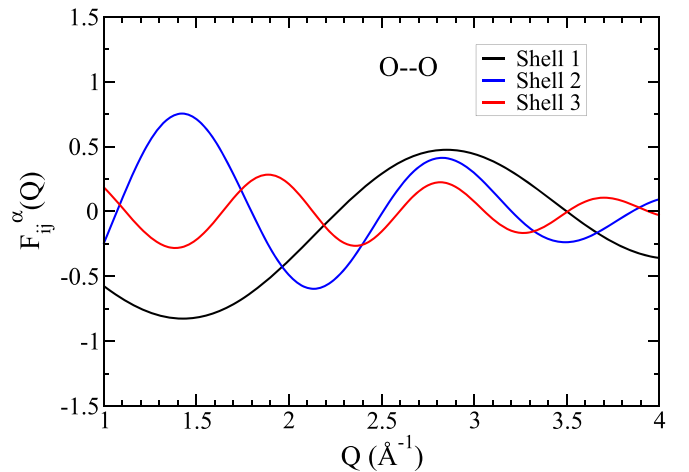FIG. 8. The shell-by-shell contributions from the first three radial shells of $G_{OO}(r)$ to $F_{OO}(Q)$ for $\alpha = 1$, 2, 3. The maxima associated with the principal peak appear near 2.8 Å^{-1}.
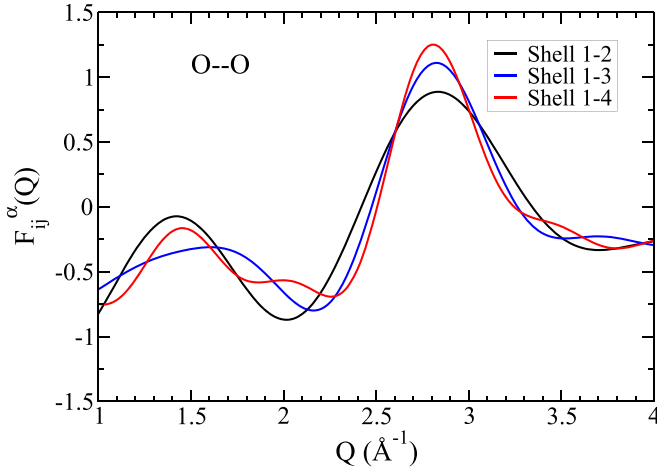
FIG. 9. The buildup of the FSDP and the principal peak near 1.5 and 2.8 Å^{-1}, respectively, from small corrections originating from the third and fourth radial shells of O–O correlations.

of the contribution from distant radial shells can be seen in Fig. 9, where the intensities obtained from the first two, first three and first four radial shells of O–O pair correlations are presented. It is apparent from Fig. 9 that the first two shells can produce the intensity and shape of the FSDP and the principal peak [in $F_{OO}(Q)$] almost correctly in the vicinity of 1.5 and 2.8 Å^{-1}, respectively. The contributions from the third and fourth shells then refine the shape of the intensity curve and add small corrections to the intensity and position of the FSDP and the principal peak.

Similar observations can be made for $F_{SiSi}(Q)$ as well. The results for this case are plotted in Figs. 10 and 11. An inspection of the plots in Fig. 10 suggests that, although the individual contributions from the first three shells of $G_{SiSi}(r)$ are not negligible in magnitude, the resultant contribution is quite small near the FSDP. This is evident from Fig. 11, where
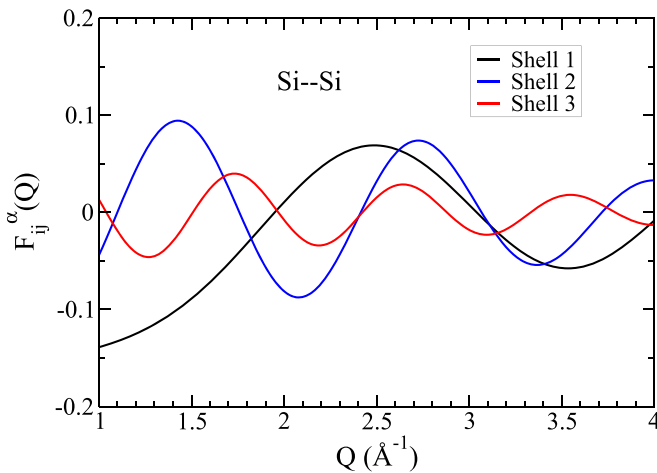

FIG. 10. The contribution to the FSDP and the principal peak from the first three individual radial shells of Si–Si correlations. The radial correlations from the second and third shells almost cancel each other, leaving behind a small net contribution from the first three shells.
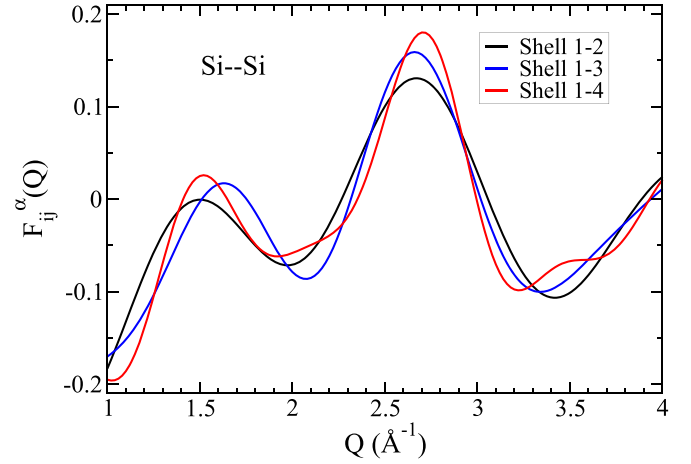

FIG. 11. The evolution of the intensity of $F_{SiSi}(Q)$ in the vicinity of the FSDP and the principal peak with an increasing number of radial shells. The plots show the contributions from the first two, first three, and first four radial shells of Si–Si correlations.

$F_{SiSi}(Q)$ is found to be considerably smaller (by a factor of about 10) than its Si–O and O–O counterparts in the vicinity of the FSDP. The neutron-weighted Si–Si correlations thus provide only a small correction to the resultant position and the intensity of the FSDP in a-SiO$_2$. This statement also applies to the principal peak to a lesser extent, where the peak height near 2.7 Å^{-1} (in Fig. 11) can be seen to increase by a small amount as the radial correlations from the third and fourth shells are taken into account.

We conclude this section by making the following remarks. Firstly, the FSDP in $F_{OO}(Q)$ is primarily determined by neutron-weighted atomic correlations originating from the first two radial shells of $G_{OO}(r)$ involving a length scale of about 6 Å. The information from the third and fourth shells then adds perturbative corrections to the intensity and shape of the FSDP. By contrast, the principal peak in $F_{OO}(Q)$ involves contributions from the first three shells with atomic correlations extending up to 9 Å. The inclusion of radial information from the fourth shell makes a small correction to the height/intensity of the principal peak. Secondly, the Si–O correlations from all the four shells (extending up to 10 Å) contribute to the intensity of the FSDP in $F_{SiO}(Q)$. With the exception of the first shell, each of the remaining three shells produces a peak in the scattering region of 1.2–1.85 Å^{-1}. These peaks combine with the minima from the second, third, and fourth (not shown in Fig. 6) shells to form the FSDP near 1.5 Å^{-1}. The involvement of the first shell is to provide a background correction to the FSDP. Thirdly, the principal *minimum* in $F_{SiO}(Q)$ in the vicinity of 2.8 Å^{-1} largely depends on the radial correlations from the first three shells, which are supplemented by a small correction from the fourth shell. This minimum effectively cancels out the scattering intensity that originates from the neutron-weighted O–O pair correlations. The Si–Si correlations then provide a small but crucial contribution (of about 2 part in 10) in the vicinity of the resultant principal peak at 2.8 Å^{-1}, but its contribution toward the intensity of the FSDP is practically negligible (cf. Figs. 5 and 11).

E. Intensity of the FSDP and the principal peak: A Gaussian approximation

Having numerically verified the approximate positions of the FSDP and the principal peak, and noting the importance of contributions from different partial components of the structure factor to the FSDP, we now obtain an analytical expression for the intensity of $F_{ij}^{\alpha}(Q)$ that arises from a given shell. Earlier, in Sec. III C, we have shown that the approximate position of the peaks in $F_{ij}^{\alpha}(Q)$, originating from a given radial shell, can be obtained by placing a sufficiently narrow distribution or a δ function at the center of the radial shell. However, the calculation of the intensity of the FSDP (or any diffraction peaks in general) requires a more sophisticated approach. To this end, the δ-function approximation can be significantly improved by replacing the δ function with a more realistic distribution, which can be represented by a linear combination of suitable radial basis functions. Assuming that the individual radial shells of $g_{ij}(r)$ are Gaussian representable [61], one can approximate the intensity due to the αth shell from Eq. (9) as

$$F_{ij}^{\alpha}(Q) = \frac{B_{ij}}{Q} \int_{R_{\alpha}} \left[r\, g_{ij}^{\alpha}(r) - r \right] \sin Qr\, dr$$

$$\approx \frac{B_{ij}}{Q} \left[\int_{R_{\alpha}} \sum_n r f_n^{\alpha} \sin Qr\, dr - \int_{R_{\alpha}} r \sin Qr\, dr \right]$$

$$\approx \frac{B_{ij}}{Q} \left[\sum_n I_n^{\alpha} - I_0 \right], \tag{10}$$

where $B_{ij} = 4\pi \rho_0 \omega_{ij}$, the symbol $\int_{R_{\alpha}}$ indicates that the integration is to be carried out from R_{α} to $R_{\alpha+1}$, and $g_{ij}^{\alpha}(r)$ can be expressed as a linear combination of Gaussian functions $f_n^{\alpha}(r)$,

$$g_{ij}^{\alpha}(r) = \sum_{n=1}^{m} f_n^{\alpha}(r) = \sum_{n=1}^{m} a_{\alpha n}\, e^{-b_{\alpha n}(r - c_{\alpha n})^2}. \tag{}$$

In general, the radial distribution of atoms in the first shell of $g_{ij}(r)$, which is not symmetric [55], can be well approximated by using a few Gaussian functions but the distant shells require several Gaussian functions in order to produce the distribution accurately within the region of R_{α} and $R_{\alpha+1}$ with correct boundary conditions. An analytical expression for $F_{ij}^{\alpha}(Q)$ can be obtained by evaluating the integrals in Eq. (10). The first integral is of the type

$$I_n = a_n \int_{x_1}^{x_2} x\, e^{-b_n(x - c_n)^2} \sin Qx\, dx, \tag{11}$$

which cannot be evaluated analytically in a closed form without the use of error functions. However, it is possible to choose a suitable set of narrow Gaussian functions f_n^{α}, which are characterized by large b_n, such that the functions decay to zero sufficiently fast before they reach the boundary points x_1 and x_2. This can be achieved by ensuring that all b_n satisfy the condition [62]

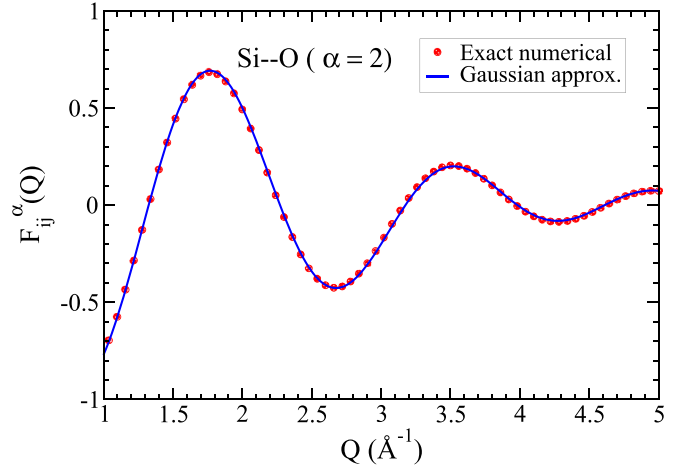$$\min[x_2 - c_n, c_n - x_1] \gg \frac{1}{\sqrt{b_n}}. \tag{12}$$

FIG. 12. The partial structure factor $F_{SiO}^{\alpha}(Q)$ for the second shell ($\alpha = 2$) obtained from exact numerical calculations (red circles) and the Gaussian approximation (blue line) using Eq. (10).

Under this condition, it is possible to obtain an analytical expression for I_n in Eq. (11). The calculation of I_n is presented in the Appendix. The second integral I_0, involving $r \sin Qr$, can be analytically calculated. The two integrals can be written as

$$I_n = a_n \sqrt{\frac{\pi}{4b_n}}\, e^{-\frac{Q^2}{4b_n}} \left[2c_n \sin Qc_n + \frac{Q \cos Qc_n}{b_n} \right] \tag{13}$$

and

$$I_0 = \left[\frac{\sin Qr - Qr \cos Qr}{Q^2} \right]_{R_{\alpha}}^{R_{\alpha+1}}. \tag{14}$$

An analytical expression for $F_{ij}^{\alpha}(Q)$ is thus obtained by substituting the results from Eqs. (13) and (14) to Eq. (10) for the αth radial shell that ranges from R_{α} to $R_{\alpha+1}$. The Gaussian parameters (a_n, b_n, c_n), where b_n satisfies the condition in Eq. (12), for a given α can be obtained by fitting the functions with the corresponding $g_{ij}^{\alpha}(r)$. It may be noted that the Gaussian representation of distant radial shells beyond the first shell is highly nontrivial due to the presence of sharp cutoffs of $g_{ij}^{\alpha}(r)$ with finite values at $r = R_{\alpha}$ and $R_{\alpha+1}$. The existence of finite values of $g_{ij}^{\alpha}(r)$ at the boundaries require that the Gaussian coefficients b_n—especially those associated with the Gaussians functions centered near the boundary—must be sufficiently large for Eq. (13) to be valid. In this study, we have employed a constrained Monte Carlo approach to obtain the desired values of b_n that simultaneously reproduce $g_{ij}^{\alpha}(r)$ within the radial region of interest and satisfy the inequality in Eq. (12) for all n.

The efficacy of the Gaussian approximation can be examined by comparing the results obtained from Eq. (10) with those from direct numerical calculations using the radial range of the shells given in Table III. Figures 12 and 13 show the results for $F_{SiO}(Q)$ for $\alpha = 2$ and 3, respectively. It is evident from the figures that the Gaussian approximation can accurately reproduce the exact numerical results. The contributions to the FSDP and the principal peak are correctly obtained from Eq. (10) for the second and third shells. Likewise, the results for the Gaussian approximation of $F_{OO}(Q)$ in Figs. 14 and 15, for $\alpha = 2$ and 3, respectively, closely
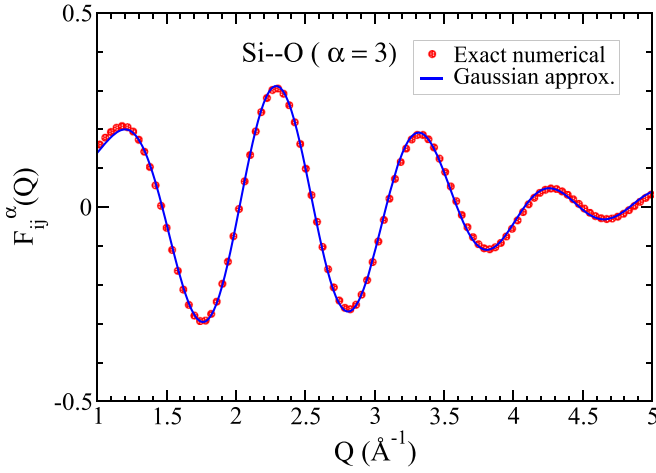
FIG. 13. $F_{\mathrm{SiO}}^{\alpha}(Q)$, for $\alpha = 3$, obtained from exact numerical calculations (red circles) and the Gaussian approximation (blue line).
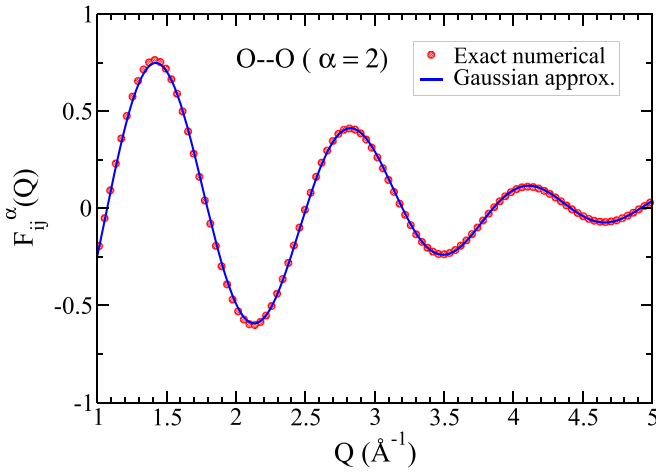

FIG. 14. A comparison of $F_{\mathrm{OO}}^{\alpha}(Q)$, obtained from exact numerical calculations (red circles), with that from the Gaussian approximation (blue line) for $\alpha = 2$.
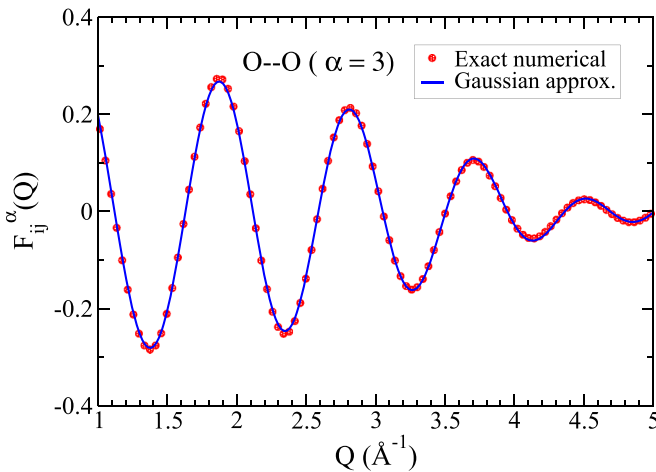

FIG. 15. A comparison of the partial structure factor of O–O pairs obtained from exact numerical calculations (red circles) and that from the Gaussian approximation (blue line) for the third shell ($\alpha = 3$).
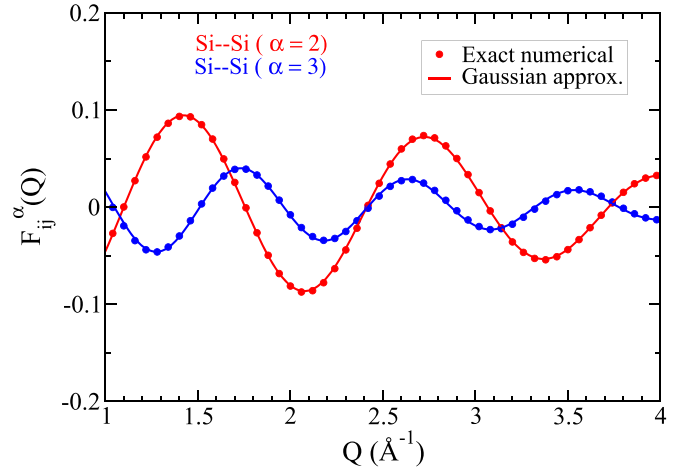

FIG. 16. The partial structure factor $F_{\mathrm{SiSi}}(Q)$ for the second (red) and third (blue) shells obtained from the semi-analytical Gaussian approximation (line) and exact numerical calculations (filled circle).

match with those from direct numerical calculations. A similar observation applies to Fig. 16, where the intensity plots of $F_{\mathrm{SiSi}}(Q)$ for $\alpha = 2, 3$ are presented. The diffraction intensity obtained from Eq. (10) using the Gaussian approximation of the (partial) pair-correlation functions and the positions of the FSDP and the principal peak estimated from Eq. (8) provide a complete picture of the origin and structure of the FSDP and the principal peak in terms of the real-space two-body distributions of silicon and oxygen atoms in the radial shells of a-SiO$_2$.

IV. CONCLUSIONS

In this paper, we have studied the origin and structure of the FSDP in a-SiO$_2$ with particular emphasis on the role of chemical and radial ordering between Si–Si, Si–O, and O-O pairs. The study leads to the following observations.

An examination of the partial structure factors of a-SiO$_2$ shows that neutron-weighted Si–O and O–O pair correlations on the length scale of 5–8 Å contribute mostly to the formation of the FSDP, whereas Si–Si correlations (from the third and fourth shells) provide only small corrections to the peak position and the intensity in the vicinity of the peak. The latter is consistent with the relatively weak neutron-weighted Si–Si pair correlations, which are found to be approximately ten times smaller than the corresponding values of Si–O and O–O correlations in the respective PCFs.

An approximate relationship between the position of the FSDP (in the partial structure factors) and the radial peak positions (in the corresponding partial PCFs) is obtained from a δ-function approximation of the structure-factor integral involving $G_{ij}(r)$. The results from this approximation are verified using numerical and semi-analytical calculations. A natural corollary of the results is that the FSDP is found to be sensitive to the pair correlations arising from a few specific radial shells. In particular, the first two shells of O–O pairs, extending as far as 6 Å, and the first three shells of Si–O pairs, with atomic correlations of up to 7 Å, are observed to play a significant role in forming the position and the

intensity of the FSDP in a-SiO$_2$. By contrast, the shape of the intensity curve near the FSDP is perturbatively modified by radial correlations originating from the remaining shells of Si–O and O–O pairs. These results are consistent with those obtained from using the continuous wavelet transform [24] of the PCFs showing that Si–O–Si–O (i.e, the second shell of Si–O pairs) and O–Si–O–Si–O (i.e., the second shell of O–O pairs) correlations contribute significantly in the formation of the FSDP in a-SiO$_2$. Likewise, the principal peak is found to depend mostly on the contribution from the Si–O and O–O pairs, and a small contribution from Si–Si pairs. The positive contribution from the O–O pairs and the negative contribution from the Si–O pairs near the principal peak competes with each other and largely cancels out. The final position and intensity of the principal peak is thus determined by the resultant contribution of Si–O and O–O pairs, and a small but nontrivial contribution of Si–Si pairs.

The study yields an accurate semi-analytical expression for the diffraction intensity of binary glasses originating from a given radial shell of the partial PCFs using a Gaussian approximation of the latter. The validity of the approximation is confirmed by directly comparing the results with those from exact numerical calculations. The approximation is independent of the nature of amorphous solids and it can be applied to both elemental and multi-component systems. The expression is found to be particularly useful for a complete characterization of the contributions emanating from each radial shell (of the PCFs) to the FSDP, and to obtain quantitative values of relevant radial length scales that form the basis of medium-range ordering in a-SiO$_2$. The results can be readily generalized and employed to other network glasses.

APPENDIX: APPROXIMATION OF $\int_a^b rg(r) \sin Qr \, dr$

In this Appendix, we obtain an approximate analytical expression for the integral above when the function $g(r)$ is Gaussian representable and it satisfies a certain condition. Expressing $g(r)$ as a linear combination of Gaussian functions, the integral can be written as

$$I = \sum_{i=1}^n \int_a^b r a_i \, e^{-b_i(r-c_i)^2} \sin Qr \, dr = \sum_{i=1}^n a_i I_i,$$

where the coefficients (a_i, b_i, c_i) parametrize the Gaussian basis sets. Substituting $y = r - c_i$ and expanding $\sin[Q(y + c_i)]$, one obtains

$$I_i = I_i^{(1)} + I_i^{(2)} + I_i^{(3)} + I_i^{(4)},$$

where

$$I_i^{(1)} = \sin Qc_i \int_{r_1}^{r_2} y \, e^{-b_i y^2} \cos Qy \, dy,$$

$$I_i^{(2)} = \cos Qc_i \int_{r_1}^{r_2} y \, e^{-b_i y^2} \sin Qy \, dy,$$

$$I_i^{(3)} = c_i \sin Qc_i \int_{r_1}^{r_2} e^{-b_i y^2} \cos Qy \, dy,$$

$$I_i^{(4)} = c_i \cos Qc_i \int_{r_1}^{r_2} e^{-b_i y^2} \sin Qy \, dy. \quad \text{(A1)}$$

The upper and lower limits of the integrals in (A1) are given by $r_1 = a - c_i$ and $r_2 = b - c_i$, respectively. In general, the integrals in Eq. (A1) cannot be expressed in a closed form without using error functions. However, if the value of b_i can be chosen in such a way that $b_i r_0^2 \gg 1$, where $r_0 = \min(|a - c_i|, |b - c_i|)$, then the function $\exp(-b_i y^2)$ inside the integrals decays sufficiently rapidly within the interval $[a - c_i, b - c_i]$ and the upper and lower limits of the integrals can be replaced by $+\infty$ and $-\infty$, respectively. Under this condition, the odd integrals vanish and one is left with

$$I_i = I_i^{(2)} + I_i^{(3)} \approx \cos Qc_i \int_{-\infty}^\infty y \, e^{-b_i y^2} \sin Qy \, dy$$

$$+ c_i \sin Qc_i \int_{-\infty}^\infty e^{-b_i y^2} \cos Qy \, dy. \quad \text{(A2)}$$

Equation (A2) involves two standard integrals, which are given by

$$\int_{-\infty}^\infty e^{-b_i y^2} \cos Qy \, dy = \sqrt{\frac{\pi}{b_i}} e^{-\frac{Q^2}{4b_i}}$$

and

$$\int_{-\infty}^\infty y e^{-b_i y^2} \sin Qy \, dy = \frac{Q}{2b_i} \sqrt{\frac{\pi}{b_i}} e^{-\frac{Q^2}{4b_i}}.$$

Collecting all the results, the original integral I can be approximated as

$$I \approx \sum_i^n a_i \sqrt{\frac{\pi}{4b_i}} e^{-\frac{Q^2}{4b_i}} \left[2c_i \sin Qc_i + \frac{Q \cos Qc_i}{b_i} \right]. \quad \text{(A3)}$$

Writing $b_i = 1/2\sigma_i^2$, the condition of validity of the result in Eq. (A3) can be stated as $\sqrt{2}\sigma_i \ll r_0 = \min(|a - c_i|, |b - c_i|)$ for all b_i, c_i, and (a, b). The validity of this expression has been verified by numerical experiments.

[1] A. C. Wright, R. A. Hulme, D. I. Grimley, R. N. Sinclair, S. W. Martin, D. L. Price, and F. L. Galeener, The structure of some simple amorphous network solids revisited, J. Non-Cryst. Solids **129**, 213 (1991).

[2] A. C. Wright, Neutron scattering from vitreous silica. V. The structure of vitreous silica: What have we learned from 60 years of diffraction studies?, J. Non-Cryst. Solids **179**, 84 (1994).

[3] S. R. Elliott, Medium range structural order in covalent amorphous solids, Nature (London) **354**, 445 (1991).

[4] P. S. Salmon, The structure of tetrahedral network glass forming systems at intermediate and extended length scales, J. Phys.: Condens. Matter **19**, 455208 (2007).

[5] Z. Zhang and W. Kob, Revealing the three-dimensional structure of liquids using four-point correlation functions, Proc. Natl. Acad. Sci. USA **117**, 14032 (2020).

[6] Q. Zhou, Y. Shi, B. Deng, T. Du, L. Guo, M. M. Smedskjaer, and M. Bauchy, Revealing the medium-range structure of

glassy silica using force-enhanced atomic refinement, J. Non-Cryst. Solids **573**, 121138 (2021).

[7] R. Shi and H. Tanaka, Distinct signature of local tetrahedral ordering in the scattering function of covalent liquids and glasses, Sci. Adv. **5**, eaav3194 (2019).

[8] A. Uhlherr and S. R. Elliott, Generation of the first sharp diffraction peak by extended-range ordering of atoms and voids in amorphous silicon, Philos. Mag. B **71**, 611 (1995).

[9] D. Dahal, H. Warren, and P. Biswas, On the origin and structure of the first sharp diffraction peak of amorphous silicon, Physica status solidi (b) **258**, 2000447 (2021).

[10] Y. Inamura, Y. Katayama, W. Utsumi, and K.-I. Funakoshi, Transformations in the intermediate-range structure of SiO_2 glass under high pressure and temperature, Phys. Rev. Lett. **93**, 015501 (2004).

[11] S. Susman, K. J. Volin, D. G. Montague, and D. L. Price, Temperature dependence of the first sharp diffraction peak in vitreous silica, Phys. Rev. B **43**, 11076 (1991).

[12] S. Susman, K. J. Volin, D. L. Price, M. Grimsditch, J. P. Rino, R. K. Kalia, P. Vashishta, G. Gwanmesia, Y. Wang, and R. C. Liebermann, Intermediate-range order in permanently densified vitreous SiO_2: A neutron-diffraction and molecular-dynamics study, Phys. Rev. B **43**, 1194 (1991).

[13] A. Fischer-Colbrie, A. Bienenstock, P. H. Fuoss, and M. A. Marcus, Structure and bonding in photodiffused amorphous $Ag-GeSe_2$ thin films, Phys. Rev. B **38**, 12388 (1988).

[14] Q. Mei, C. J. Benmore, S. Sen, R. Sharma, and J. L. Yarger, Intermediate range order in vitreous silica from a partial structure factor analysis, Phys. Rev. B **78**, 144204 (2008).

[15] C. Crupi, G. Carini, M. González, and G. D'Angelo, Origin of the first sharp diffraction peak in glasses, Phys. Rev. B **92**, 134206 (2015).

[16] M. Zanatta, G. Baldi, R. S. Brusa, W. Egger, A. Fontana, E. Gilioli, S. Mariazzi, G. Monaco, L. Ravelli, and F. Sacchetti, Structural evolution and medium range order in permanently densified vitreous SiO_2, Phys. Rev. Lett. **112**, 045501 (2014).

[17] K. Tanaka, Medium-range structure in chalcogenide glasses, Jpn. J. Appl. Phys. **37**, 1747 (1998).

[18] Y. Shi, J. Neuefeind, D. Ma, K. Page, L. A. Lamberson, N. J. Smith, A. Tandia, and A. P. Song, Ring size distribution in silicate glasses revealed by neutron scattering first sharp diffraction peak analysis, J. Non-Cryst. Solids **516**, 71 (2019).

[19] P. S. Salmon, A. Zeidler, M. Shiga, Y. Onodera, and S. Kohara, Ring compaction as a mechanism of densification in amorphous silica, Phys. Rev. B **107**, 144203 (2023).

[20] P. Vashishta, R. K. Kalia, J. P. Rino, and I. Ebbsjö, Interaction potential for SiO_2: A molecular-dynamics study of structural correlations, Phys. Rev. B **41**, 12197 (1990).

[21] S. R. Elliott, The origin of the first sharp diffraction peak in the structure factor of covalent glasses and liquids, J. Phys.: Condens. Matter **4**, 7661 (1992).

[22] S. R. Elliott, Origin of the first sharp diffraction peak in the structure factor of covalent glasses, Phys. Rev. Lett. **67**, 711 (1991).

[23] J. Sarnthein, A. Pasquarello, and R. Car, Structural and electronic properties of liquid and amorphous SiO_2: An *ab initio* molecular dynamics study, Phys. Rev. Lett. **74**, 4682 (1995).

[24] T. Uchino, J. D. Harrop, S. N. Taraskin, and S. R. Elliott, Real and reciprocal space structural correlations contributing to the first sharp diffraction peak in silica glass, Phys. Rev. B **71**, 014202 (2005).

[25] K. Kobayashi, M. Okumura, H. Nakamura, M. Itakura, M. Machida, S. Urata, and K. Suzuya, Machine learning molecular dynamics reveals the structural origin of the first sharp diffraction peak in high-density silica glasses, Sci. Rep. **13**, 18721 (2023).

[26] C.Z. Tan and J. Arndt, X-ray diffraction of densified silica glass, J. Non-Cryst. Solids **249**, 47 (1999).

[27] P. H. Gaskell and D. J. Wallis, Medium-range order in silica, the canonical network glass, Phys. Rev. Lett. **76**, 66 (1996).

[28] D. L. Price, S. C. Moss, R. Reijers, M. L. Saboungi, and S. Susman, Intermediate-range order in glasses and liquids, J. Phys.: Condens. Matter **1**, 1005 (1989).

[29] C. Massobrio and A. Pasquarello, Origin of the first sharp diffraction peak in the structure factor of disordered network-forming systems: Layers or voids?, J. Chem. Phys. **114**, 7976 (2001).

[30] A. B. Bhatia and D. E. Thornton, Structural aspects of the electrical resistivity of binary alloys, Phys. Rev. B **2**, 3004 (1970).

[31] J. Blétry, Sphere and distance models for binary disordered systems, Philos. Mag. B **62**, 469 (1990).

[32] S. R. Elliott, Second sharp diffraction peak in the structure factor of binary covalent network glasses, Phys. Rev. B **51**, 8599 (1995).

[33] R. L. McGreevy, Reverse Monte Carlo modelling, J. Phys. Condens. Matter **13**, R877 (2001).

[34] A. Pandey, P. Biswas, and D. A. Drabold, Force-enhanced atomic refinement: Structural modeling with interatomic forces in a reverse Monte Carlo approach applied to amorphous Si and SiO_2, Phys. Rev. B **92**, 155205 (2015).

[35] D. Marx and J. Hutter, *Ab Initio Molecular Dynamics: Basic Theory and Advanced Methods* (Cambridge University Press, Cambridge, 2009).

[36] D. A. Drabold, P. A. Fedders, O. F. Sankey, and J. D. Dow, Molecular-dynamics simulations of amorphous Si, Phys. Rev. B **42**, 5135 (1990).

[37] D. N. Tafen and D. A. Drabold, Realistic models of binary glasses from models of tetrahedral amorphous semiconductors, Phys. Rev. B **68**, 165208 (2003).

[38] O. V. Mazurin, M. V. Streltsina, and T. P. Shvaiko-Shvaikovskaya, *Handbook of Glass Data Part A: Silica Glass and Binary Silicate Glasses* (Elsevier, Amsterdam, 1983).

[39] D. K. Limbu, S. R. Elliott, R. Atta-Fynn, and P. Biswas, Disorder by design: A data-driven approach to amorphous semiconductors without total-energy functionals, Sci. Rep. **10**, 7742 (2020).

[40] P. Biswas, R. Atta-Fynn, and D. A. Drabold, Reverse Monte Carlo modeling of amorphous silicon, Phys. Rev. B **69**, 195207 (2004).

[41] D. A. Keen and R. L. McGreevy, Structural modelling of glasses using reverse Monte Carlo simulation, Nature (London) **344**, 423 (1990).

[42] G. Opletal, T. C. Petersen, I. K. Snook, and S. P. Russo, HRMC_2.0: Hybrid reverse Monte Carlo method with silicon, carbon and germanium potentials, Comput. Phys. Commun. **184**, 1946 (2013).

[43] P. Biswas, D. N. Tafen, and D. A. Drabold, Experimentally constrained molecular relaxation: The case of glassy $GeSe_2$, Phys. Rev. B **71**, 054204 (2005).

[44] P. Biswas, R. Atta-Fynn, and D. A. Drabold, Experimentally constrained molecular relaxation: The case of hydrogenated amorphous silicon, Phys. Rev. B **76**, 125210 (2007).

[45] A. Pandey, P. Biswas, B. Bhattarai, and D. A. Drabold, Realistic inversion of diffraction data for an amorphous solid: The case of amorphous silicon, Phys. Rev. B **94**, 235208 (2016).

[46] D. K. Limbu, R. Atta-Fynn, D. A. Drabold, S. R. Elliott, and P. Biswas, Information-driven inverse approach to disordered solids: Applications to amorphous silicon, Phys. Rev. Mater. **2**, 115602 (2018).

[47] J. M. Soler, E. Artacho, J. D. Gale, A. Garciá, J. Junquera, P. Ordejón, and D. Sánchez-Portal, The SIESTA method for *ab initio* order-N materials simulation, J. Phys.: Condens. Matter **14**, 2745 (2002).

[48] N. Troullier and J. L. Martins, Efficient pseudopotentials for plane-wave calculations, Phys. Rev. B **43**, 1993 (1991).

[49] J. P. Perdew, K. Burke, and M. Ernzerhof, Generalized gradient approximation made simple, Phys. Rev. Lett. **77**, 3865 (1996).

[50] S. R. Elliott, *Physics of Amorphous Materials*, 2nd ed. (Longman, London, 1990).

[51] N. E. Cusack, *The Physics of Structurally Disordered Matter* (Adam Hilger/IOP Publishing Ltd., Bristol, 1987).

[52] G. E. Bacon, *Neutron Diffraction* (Clarendon Press, Oxford, 1975).

[53] T. E. Faber and J. M. Ziman, A theory of the electrical properties of liquid metals, Philos. Mag. **11**, 153 (1965).

[54] The use of periodic boundary conditions and finite-size models of linear dimension L leads to a lower cutoff value of $Q_{min} \approx 4\pi/L$. For $Q \approx Q_{min} \ll 1$ Å^{-1}, $S(Q)$ can be written as a polynomial in Q, where the coefficients of the polynomial are given by the power moments of $G(r)$. These moments are sensitive to numerical noise in $G(r)$ at large distances, causing artifacts to appear in $S(Q)$ near Q_{min}.

[55] P. A. V. Johnson, A. C. Wright, and R. N. Sinclair, Neutron scattering from vitreous silica II. Twin-axis diffraction experiments, J. Non-Cryst. Solids **58**, 109 (1983).

[56] L. C. Erhard, J. Rohrer, K. Albe, and V. L. Deringer, A machine-learned interatomic potential for silica and its relation to empirical models, npj Comput. Mater. **8**, 90 (2022).

[57] R. L. Mozzi and B. E. Warren, The structure of vitreous silica, J. Appl. Cryst. **2**, 164 (1969).

[58] Assuming $g(r)$ is Gaussian representable, the peak positions in $g(r)$ and $r^2 g(r)$ are separated by $\delta r_n \approx 2\sigma_n^2/r_n$, where r_n and σ_n are the Gaussian peak and width of the n-th radial shell of $g(r)$, respectively. Thus, the approximation holds for $\sigma_n \ll r_n$, which is always satisfied by a well-defined radial shell. The presence of linear and quadratic shifts of r in $G(r)$ and $rG(r)$, respectively, slightly modify this estimate.

[59] The maximal value of the perturbative correction is obtained for $n = 1$ and $r_{Si-O} = 1.65$ Å in Eq. (7). This gives a value of 0.077 Å^{-1} for a maximum and 0.128 Å^{-1} for a minimum. For distant radial peaks and $n > 1$, the correction can be ignored.

[60] A more rigorous calculation, using the saddle-point approximation of the integral in Eq. (6), by writing $\sin(Qr) = Im\, e^{iQr}$ and $G(r)$ as a linear combination of Gaussian functions centered at radial peaks (r_k), $\sum_k a_k \exp(-b_k(r - r_k)^2)$, leads to identical values of Q_k as in Eq. (8).

[61] D. Dahal, S. R. Elliott, and P. Biswas, Extended-range order in tetrahedral amorphous semiconductors: The case of amorphous silicon, Phys. Rev. B **105**, 115203 (2022).

[62] Noting that a Gaussian function decays to almost zero at a distance of 4σ from the center, a sharper upper bound for σ^2 ($=1/2b$) can be stated as $4\sigma \leqslant \min[|x_2 - c|, |x_1 - c|]$.